# NACA

# RESEARCH MEMORANDUM

MISCELLANEOUS DIRECTIONAL-STABILITY DATA FOR SEVERAL

AIRPLANE-LIKE CONFIGURATIONS FROM ROCKET-MODEL

TESTS AT TRANSONIC SPEEDS

By Paul E. Purser and Jesse L. Mitchell

Langley Aeronautical Laboratory
Langley Field, Va.

# NATIONAL ADVISORY COMMITTEE
# FOR AERONAUTICS

## WASHINGTON

NATIONAL ADVISORY COMMITTEE FOR AERONAUTICS

RESEARCH MEMORANDUM

MISCELLANEOUS DIRECTIONAL-STABILITY DATA FOR SEVERAL

AIRPLANE-LIKE CONFIGURATIONS FROM ROCKET-MODEL

TESTS AT TRANSONIC SPEEDS

By Paul E. Purser and Jesse L. Mitchell

SUMMARY

Some approximate values of the yawing moment due to sideslip derivative for eight airplane-like configurations flown as rocket models for other purposes, at transonic speeds, have been collected and compared with the available subsonic and supersonic wind-tunnel data for the same configurations.

The comparisons of tunnel and rocket data tended to verify the magnitude of values of directional stability indicated by the rocket tests even though the rocket data were obtained by a simplified single-degree-of freedom analysis of random oscillations at low angles of attack and sideslip.

The rocket data indicated that the maximum value of the directional-stability derivative $C_{n_\beta}$ occurred at Mach numbers between 1.1 and 1.2. Although the data showed appreciable scatter because of the random nature of the oscillations, the variation of $C_{n_\beta}$ with Mach number at transonic speeds generally appeared to be fairly smooth and regular. There was some evidence in the rocket-model data of cross coupling between pitch and yaw at low lift coefficients when the frequencies in pitch and yaw approached equality.

The available data indicate little variation with Mach number of the wing-body contribution to $C_{n_\beta}$ at low lift coefficients. None of the data indicated the probability of any unusual vertical-tail-load problems at transonic speeds.

## INTRODUCTION

Several rocket models of airplane-like configurations flown by the Langley Pilotless Aircraft Research Division in investigations of drag or longitudinal stability and control have been instrumented to record lateral force. Random oscillations have appeared in the lateral-force records, in the transonic speed range, as a result of rough air or other disturbances introduced into the flights. These oscillations have been analyzed by the method presented in reference 1 to obtain approximate values of the yawing moment due to sideslip derivative. Because of the general lack of experimental data, at transonic speeds, for many of the sideslip derivatives, the effective values of directional stability calculated from the records of 13 model flights (8 airplane-like configurations) have been collected. The configurations considered have both unswept and swept wing and vertical-tail plan forms.

The directional-stability data are presented in this paper with no analysis other than comparisons with the available subsonic and supersonic wind-tunnel data for the same configurations in order to make the data more immediately available to designers.

## SYMBOLS

$C_L$      lift coefficient, $\dfrac{\text{Lift}}{qS}$

$C_n$      yawing-moment coefficient,
$$\dfrac{\text{Yawing moment about center of gravity}}{qSb}$$

$S$      wing area, sq ft

$b$      wing span, ft

$\bar{c}$      wing mean aerodynamic chord, ft

$q$      dynamic pressure, $\dfrac{\gamma}{2}pM^2$, lb/sq ft

$p$      static pressure, lb/sq ft

$M$      Mach number

| $\gamma$ | specific heat ratio for air, 1.4 |
|---|---|

$\beta$       sideslip angle, deg

$C_{n_\beta}$       rate of change of yawing-moment coefficient with sideslip angle per deg

$C_{n_\beta}{}^*$       effective value of $C_{n_\beta}$, calculated from single-degree-of-freedom equation of reference 1, $C_{n_\beta}{}^* = 0.688\ \dfrac{I_Z}{qSbP^2}$, per deg

$I_Z$       moment of inertia in yaw, slug-ft$^2$

$P$       period of yawing motion as indicated by lateral accelero-meter reading (lateral force), sec

## MODELS AND INSTRUMENTATION

The models from which data were obtained had been propelled to various maximum speeds in free air by various combinations of internal and external solid-propellant rockets. Table I presents the principal geometric characteristics of all the models considered and three-view drawings of each model are presented with the $C_{n_\beta}{}^*$ data in the data figures. Additional data on the construction and propulsion systems of most of the models may be obtained from references 2 to 5.

Instrumentation common to all models and pertinent to the present study consisted of a telemetered lateral accelerometer providing con-tinuous records of lateral force against time. Values of Mach number and dynamic pressure were computed from various combinations of telemetered static-pressure data, telemetered total-pressure data, velocity data from a Doppler radar unit, flight-path data from an NACA modified SCR 584 tracking radar, and atmospheric data from radiosondes. Refer-ences 2 to 5 discuss the instrumentation for the models more completely.

## DATA AND ANALYSIS PROCEDURES

The primary data were obtained as continuous-line records of lateral force against time. Oscillations due to rough air or other unidenti-fiable sources appeared in these records. The oscillations were random in nature and their magnitudes generally were less than ±10 percent of the calibrated instrument range. The magnitudes generally corresponded

to oscillations in sideslip of less than $\pm 1°$. The periods of the oscillations were obtained by measuring the time required for the occurrence of one or more complete cycles. The random nature and small amplitude of the oscillations induced appreciable scatter in the measurements of period. No attempt was made to fair a curve of period against Mach number to reduce the scatter because, for most cases, insufficient data were available from any one flight to define such a curve adequately.

The conversion of the period data to values of $C_{n_\beta}{}^*$ was made by using the single-degree-of-freedom expression from reference 1 (see the symbol list). In order to show the validity of this single-degree-of-freedom approximation for airplane configurations similar to the models considered herein, some "true" and "effective" values of $C_{n_\beta}$ are compared in figure 1. The true values of $C_{n_\beta}$ are those used along with the best available measured and estimated values of all the directional-stability derivatives to calculate the period of sideslip oscillation for four airplanes in the flaps- and gear-up condition by using the complete equations of motion (ref. 6 to 8 and unpublished data). The effective values of $C_{n_\beta}$ are those calculated by the single-degree-of-freedom procedure by using the period obtained from the complete equations. The comparison in figure 1 shows that, in most cases, the true and effective values of $C_{n_\beta}$ agree within $\pm 0.0005$.

## RESULTS AND DISCUSSION

### Basic Data

The values of $C_{n_\beta}{}^*$ calculated from the rocket-flight data are presented in figures 2 to 9 for models 1 to 8. Also presented in figures 2 to 9 are three-view drawings of each model and the available wind-tunnel data on $C_{n_\beta}$ for each model taken from references 6 to 14 and various unpublished sources. The wind-tunnel values of $C_{n_\beta}$ are presented for the complete models and, where possible, for component parts of the models. All the wind-tunnel values of $C_{n_\beta}$ have been transferred to the flight-model center-of-gravity location. Each curve

or group of data points in figures 2 to 9 is labeled with some one, or combination, of the letters W, B, H, and V to indicate the components of which the model consisted when the data were obtained.  The meanings of the letters are:

W          wing

B          body, including canopy where shown in sketch

H          horizontal tail

V          vertical tail (vee tail for model 7)

      Other information of interest for particular models is given in table II.

## General Trends

      Agreement with tunnel data.- The values of $C_{n_\beta}$* for the rocket models shown in figures 2 to 9 generally agree well in magnitude with test data or reasonable extrapolations of test data from subsonic and supersonic wind-tunnel tests.  There is one apparent exception to this agreement, model 8.  For model 8 there were the following differences between the wind-tunnel and rocket models:  (a) The rocket model had longer fuselage ahead of wing, (b) the rocket model had smaller base (greater boattail on rear of fuselage), and (c) the rocket model was flown with aluminum-shell fuselage and magnesium vertical surface at nearly sea level static pressure, whereas the tunnel model had steel surfaces and a steel reinforced body and was tested at less than sea-level static pressure.  All these differences would be expected to result in lower values of $C_{n_\beta}$ for the rocket model.  Quantitatively, the aeroelastic loss has been estimated and the magnesium vertical tail on the rocket model is felt to have been about 85 and 70 percent effective, as compared to the steel tail, at Mach numbers of 0.85 and 1.4, respectively.  By using this loss in tail effectiveness and a value of $C_{n_\beta}$ for fuselage as estimated from reference 15, most of the difference between rocket model $C_{n_\beta}$ and tunnel model $C_{n_\beta}$ can be explained.

      Complete-model $C_{n_\beta}$ at transonic speeds.- The variations of $C_{n_\beta}$* with Mach number in the transonic range appear to be generally regular with peak values occurring at transonic speeds as is usually the case for the lift-curve slope of finite-aspect-ratio airfoils.  Although the data are very scattered, probably because of the random nature of the

oscillations and possibly because of nonlinearities at small angles of sideslip, the rocket models all appeared to have maximum values of $C_{n_\beta}*$ at Mach numbers between 1.1 and 1.2. The maximum lift-curve slope for finite-aspect-ratio airfoils (refs. 16 and 17) generally occurs quite close to M = 1. The rearward shift in the aerodynamic center which occurs in the transonic range, however, is usually not complete at M = 1. This rearward movement of the aerodynamic center at M > 1 probably is the cause of the maximum value of $C_{n_\beta}*$ occurring at M = 1.1 to 1.2 instead of at M = 1 as for lift-curve slopes.

Pitch-yaw cross coupling.- The data for model 5 showed a reduction in $C_{n_\beta}*$ at Mach numbers between 1.0 and 1.2 both with and without external stores installed. The reason for this apparent decrease is not known but it is probable that the $C_{n_\beta}*$ values in the Mach number range between M = 0.85 and 0.98 are erroneously high because of cross coupling with an oscillation in pitch that is known to have occurred simultaneously with, and at the same frequency as, the lateral oscillation. The wind-tunnel data tend to support this explanation as does the rocket-model peak in $C_{n_\beta}*$ at M = 1.2 which is consistent with the data for the other models. The rocket-model data near M = 1.3, which agree with the wind-tunnel data, were also obtained when the model was oscillating in both pitch and yaw but not at equal frequencies in the two planes, thus, the cross coupling, if any, was appreciable only at subsonic speeds where the pitch and yaw frequencies were approximately equal for this model. Examination of the basic data records showed that equal-frequency pitch and yaw oscillations occurred for the following models and Mach numbers:

| Model | Mach number | Figure |
|-------|-------------|--------|
| 1 | 1.21 to 1.23 | 2 |
| 4 | 1.17 | 5 |
| 5 | 0.85 to 0.98 | 6 |
| 8 | 0.88 to 1.05 | (Not presented) |

These equal-frequency oscillations generally occurred at values of $C_L$ between -0.1 and 0.1. The values of $C_{n_\beta}*$ for the above models and Mach numbers may be erroneous and should therefore not be given much weight in estimating the variation of $C_{n_\beta}*$ with M.

The reason for the existence of the cross-coupled oscillations is, as yet, unknown. The low lift at which the oscillations occurred and the appearance of equal pitch and yaw frequencies indicate that the cross coupling is not the high-angle-of-attack type treated in reference 18 nor

the low-angle type encountered in some research-airplane flight tests where the pitch frequency was twice the yaw frequency (ref. 19).

Fuselage $C_{n_\beta}$ at transonic speeds.- There are no data to indicate directly the variation of the fuselage contribution to $C_{n_\beta}$ with Mach number at transonic speeds except the wing-off data from reference 15. It might be expected that slender bodies would show no marked variations of $C_{n_\beta}$ with Mach number and both the rocket data (ref. 15) and the wind-tunnel data for models 2, 3, 4, and 5 tend to substantiate this belief. The magnitudes of the values of tail-off $C_{n_\beta}$ generally agree reasonably well with estimates based on the data and procedures of references 20 and 21.

Vertical-tail loads.- None of the data for models 1 to 8, all of which had fairly thin stabilizing surfaces, indicated any radical losses in $C_{n_\beta}$ at transonic speeds. Thus, no unusual vertical-tail loads would be expected to occur at Mach numbers near 1. Not enough is known as yet about the coupled oscillations which occurred for models 1, 4, 5, and 8 to estimate whether they would occur on the airplanes. For the models, however, the amplitudes of the coupled oscillations were not appreciably different from those of the other oscillations. Therefore the possible existence of such coupled oscillations for the airplane is felt to be more of a handling-qualities problem than a tail-loads problem.

CONCLUDING REMARKS

Comparisons of the yawing moment due to sideslip derivative $C_{n_\beta}$ values from wind-tunnel data and from single-degree-of-freedom analyses of random oscillations in rocket-model data for several airplane-like configurations show fair agreement. The rocket-model data generally show fairly smooth variations of effective $C_{n_\beta}$ with Mach number and maximum values of effective $C_{n_\beta}$ occurred in the Mach number range between 1.1 and 1.2. There was some evidence in the rocket tests of cross coupling between pitch and yaw at low lift coefficients when the frequencies in pitch and yaw approached equality. The data indicated very little

variation with Mach number of the wing-body contribution to $C_{n_\beta}$ at low lift. None of the data indicated the probability of any unusual vertical-tail-load problems at transonic speeds.


Langley Aeronautical Laboratory
    National Advisory Committee for Aeronautics
        Langley Field, Va.

REFERENCES

1. Bishop, Robert C., and Lomax, Harvard:  A Simplified Method for
     Determining From Flight Data the Rate of Change of Yawing-Moment
     Coefficient With Sideslip.  NACA TN 1076, 1946.

2. Gillis, Clarence L., and Mitchell, Jesse L.:  Flight Tests at
     Transonic and Supersonic Speeds of an Airplane-Like Configuration
     With Thin Straight Sharp-Edge Wings and Tail Surfaces.
     NACA RM L8K04a, 1949.

3. D'Aiutolo, Charles T., and Mason, Homer P.:  Preliminary Results of
     the Flight Investigation Between Mach Numbers of 0.80 and 1.36 of
     a Rocket-Powered Model of a Supersonic Airplane Configuration
     Having a Tapered Wing With Circular-Arc Sections and 40° Sweep-
     back.  NACA RM L50H29a, 1950.

4. Parks, James H., and Mitchell, Jesse L.:  Longitudinal Trim and Drag
     Characteristics of Rocket-Propelled Models Representing Two Air-
     plane Configurations.  NACA RM L9L22, 1950.

5. Alexander, Sidney R.:  Flight Investigation To Determine the
     Aerodynamic Characteristics of Rocket-Powered Models Representative
     of a Fighter-Type Airplane Configuration Incorporating an Inverse-
     Taper Wing and a Vee Tail.  NACA RM L8G29, 1948.

6. Queijo, M. J., and Michael, W. H., Jr.:  Analysis of the Effects of
     Various Mass, Aerodynamic, and Dimensional Parameters on the
     Dynamic Lateral Stability of the Douglas D-558-2 Airplane.
     NACA RM L9A24, 1949.

7. Queijo, M. J., and Goodman, Alex:  Calculations of the Dynamic
     Lateral Stability Characteristics of the Douglas D-558-II Airplane
     in High-Speed Flight for Various Wing Loadings and Altitudes.
     NACA RM L50H16a, 1950.

8. Michael, W. H., Jr., and Queijo, M. J.:  Analysis of the Dynamic
     Lateral Stability Characteristics of the Bell X-2 Airplane As
     Affected by Variations in Mass, Aerodynamic, and Dimensional
     Parameters.  NACA RM L9G13, 1949.

9. Bauer, C. R., and Kleckner, H. F.:  Supersonic Dynamic Lateral
     Stability of the MX-656 Airplane (Design No. 39C).  Rep.
     No. SM-13061, Douglas Aircraft Co., Inc., July 21, 1947.

10. Bauer, C. R., and Kleckner, H. F.:  Subsonic Dynamic Lateral Stability of the MX-656 Airplane (Design No. 39C).  Rep. No. SM-13196, Douglas Aircraft Co., Inc., Feb. 6, 1948.

11. Spearman, M. Leroy, and Robinson, Ross B.:  The Aerodynamic Characteristics of a Supersonic Aircraft Configuration With a 40° Sweptback Wing Through a Mach Number Range From 0 to 2.4 As Obtained From Various Sources.  NACA RM L52A21, 1952.

12. Ross, Don H.:  Wind Tunnel Tests on Republic Aviation Corporation Model MX-809, Second Series.  M.I.T. Wind Tunnel Rep. No. 745, Oct., 1946.

13. Purser, Paul E., and Spearman, M. Leroy:  Wind-Tunnel Tests at Low Speed of Swept and Yawed Wings Having Various Plan Forms. NACA TN 2445, 1951. (Supersedes NACA RM L7D23.)

14. Phelps, E. Ray, and Lazzeroni, Frank A.:  Wind-Tunnel Investigation of the Aerodynamic Characteristics of a 1/15-Scale Model of the Northrop MX-775A Missile.  NACA RM A51E28, 1951.

15. Gillis, Clarence L., and Vitale, A. James:  Wing-On and Wing-Off Longitudinal Characteristics of an Airplane Configuration Having a Thin Unswept Tapered Wing of Aspect Ratio 3, As Obtained From Rocket-Propelled Models at Mach Numbers From 0.8 to 1.4.  NACA RM L50K16, 1951.

16. Polhamus, Edward C.:  Summary of Results Obtained by Transonic-Bump Method on Effects of Plan Form and Thickness on Lift and Drag Characteristics of Wings at Transonic Speeds.  NACA RM L51H30, 1951.

17. Nelson, Warren H., and McDevitt, John B.:  The Transonic Characteristics of 17 Rectangular, Symmetrical Wing Models of Varying Aspect Ratio and Thickness.  NACA RM A51A12, 1951.

18. Stone, Ralph W., Jr.:  Estimation of the Maximum Angle of Sideslip for Determination of Vertical-Tail Loads in Rolling Maneuvers. NACA TN 2633, 1952.

19. Williams, W. C., and Crossfield, A. S.:  Handling Qualities of High-Speed Airplanes.  NACA RM L52A08, 1952.

20. Goodman, Alex:  Effects of Wing Position and Horizontal-Tail Position on the Static Stability Characteristics of Models With Unswept and 45° Sweptback Surfaces With Some Reference to Mutual Interference. NACA TN 2504, 1951.

21. Campbell, John P., and McKinney, Marion O.:  Summary of Methods for Calculating Dynamic Lateral Stability and Response and for Estimating Lateral Stability Derivatives.  NACA TN 2409, 1951.

TABLE I

MODEL GEOMETRY

| Model dimension (a) | Model number | | | | | | | |
|---|---|---|---|---|---|---|---|---|
| | 1 | 2 | 3 | 4 | 5 | 6 | 7 | 8 |
| Fuselage: | | | | | | | | |
| $l_f/b$ | 2.20 | 2.33 | 2.33 | 1.32 | 1.19 | 1.69 | 1.49 | 1.60 |
| $l_f^*/b$ | 2.79 | | | 1.16 | | | | |
| $h/b$ | 0.217 | 0.185 | 0.185 | 0.159 | | 0.200 | 0.193 | 0.114 |
| $w/b$ | 0.269 | 0.185 | 0.185 | 0.124 | | 0.200 | 0.144 | 0.114 |
| Volume/Sb | 0.193 | 0.149 | 0.149 | 0.0425 | | 0.127 | 0.075 | 0.075 |
| Vertical tail: | | | | | | | | |
| $l_t/b$ | 1.024 1.075 | 0.880 0.934 | 0.885 0.938 | 0.368 | 0.520 | 0.600 | b0.632 | 0.848 |
| $b_t/b$ | 0.246 | 0.327 | 0.359 | 0.283 | 0.298 | 0.281 | b0.66 | 0.236 |
| $S_t/S$ | 0.142 | 0.213 | 0.260 | 0.240 | 0.086 | 0.316 | b0.25 | 0.138 |
| $\Lambda c/4$, deg | 38 | 8 | 8 | 33 | 28 | 55 | b34 | 36 |
| Taper ratio | 0.30 | 0.49 | 0.50 | 0.27 | 0.26 | 0.30 | 1.0 | 0.29 |
| Average thickness ratio | 0.045 | 0.046 | 0.046 | 0.09 | 0.07 | 0.077 | b0.083 | 0.062 |
| Wing: | | | | | | | | |
| $b^2/S$ | 3.0 | 4.0 | 4.0 | 4.0 | 2.0 | 3.5 | 3.1 | 5.5 |
| $\Lambda_{c/4}$ (sweepback), deg | 16 | 8 | 8 | 40 | 46 | 35 | 37 | 46 |
| Taper ratio | 0.40 | 0.50 | 0.50 | 0.50 | 0.33 | 0.57 | 1.63 | 0.4 |
| $\bar{c}/b$ | 0.348 | 0.260 | 0.260 | 0.259 | 0.543 | 0.291 | 0.338 | 0.194 |

aDimensions are defined in data figures (figs. 2 to 9).

bModel 7 has a vee tail with 38° dihedral (see fig. 8). Dimensions shown are true view, that is, as if there were no dihedral.

TABLE II

ADDITIONAL INFORMATION

| Model number | Rocket tests | Wind-tunnel tests |
|---|---|---|
| 1 | Air flow through ducts (unpublished data); mass-flow ratio about 0.8 | Air flow through ducts (unpublished data); mass-flow ratio of about 0.85; $C_{n_\beta}$ measured at $\beta \doteq 2°$ to $5°$ and $-2°$ to $-5°$ because low Reynolds number of tunnel tests believed to have caused erroneously low $C_{n_\beta}$ at $\beta = 0°$ |
| 2 | | Tunnel tests (refs. 9 and 10) made with vertical tail on and wing off; not believed important because of low $C_L$ (<0.4) of rocket tests |
| 3 | Identical to model 2 except for 25-percent larger vertical tail | No direct tunnel test data for model 3; estimates made by multiplying $C_{n_\beta}$ contribution of model 2 tail by 1.25 |
| 4 | No rudder cutout in rocket model | Rudder cutout in one wind-tunnel model (ref. 11) believed to have caused difference between wind-tunnel values of $C_{n_\beta}$ at M = 1.6 (fig. 5); no rudder cutout on subsonic tunnel model |
| 5 | Air flow through ducts; mass-flow ratio about 0.5 | Air flow through ducts; mass-flow ratio about 0.85 |
| 6 | Vertical tail shorter in span, by 14 inches full-scale, than on airplane of reference 7 | Vertical tail shorter in span, by 14 inches full-scale, than on airplane of reference 7 |
| 7 | Only one oscillation of about 2 cycles occurred during flight | |
| 8 | Rocket model had magnesium vertical surface and aluminum-shell body | Wind-tunnel model (ref. 14) had shorter fuselage and larger base than rocket model; tunnel model was steel construction and was tested at lower dynamic pressure than rocket model |
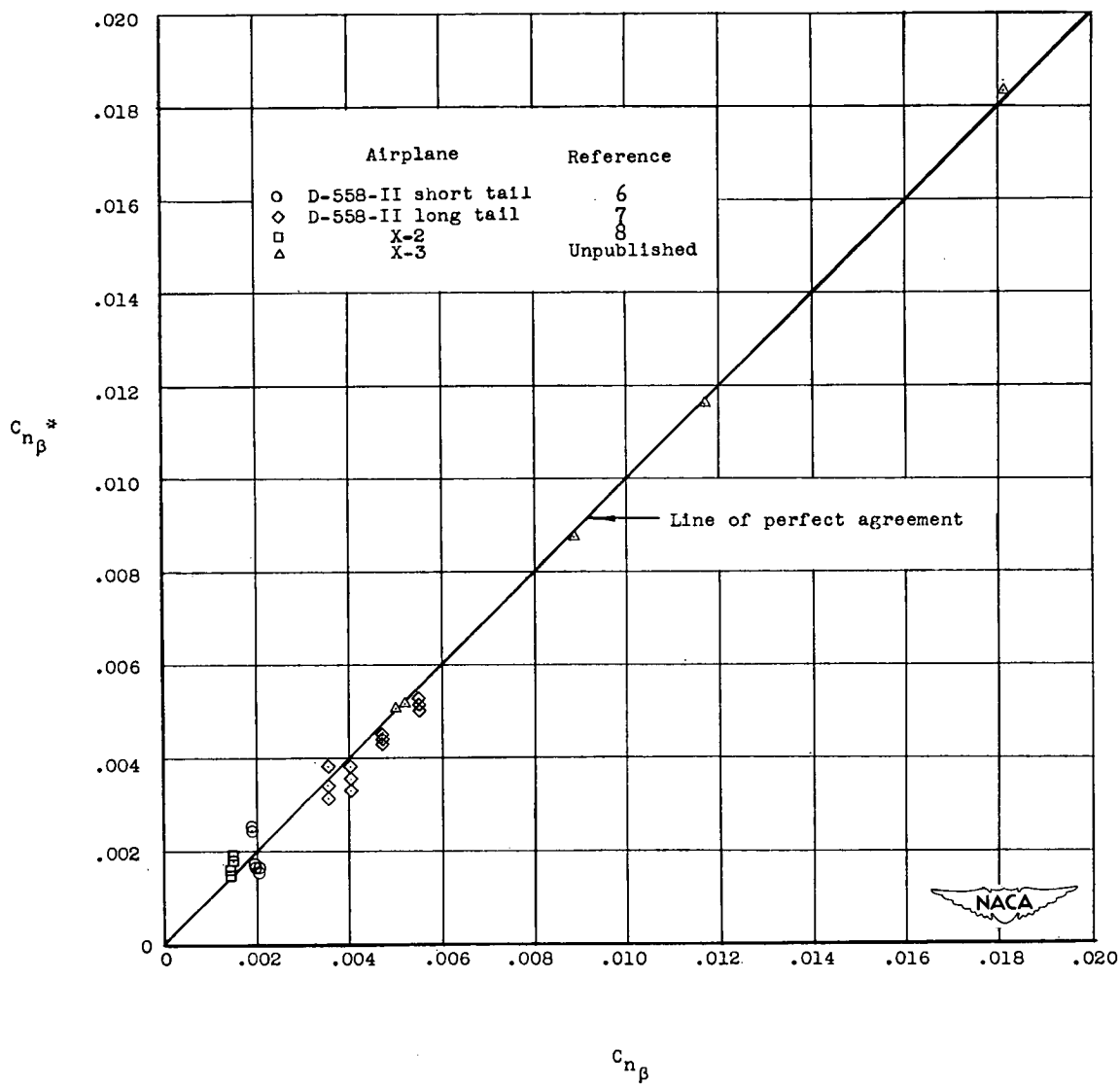
Figure 1.- Comparison of true and effective values of directional-stability derivative $C_{n_\beta}$.
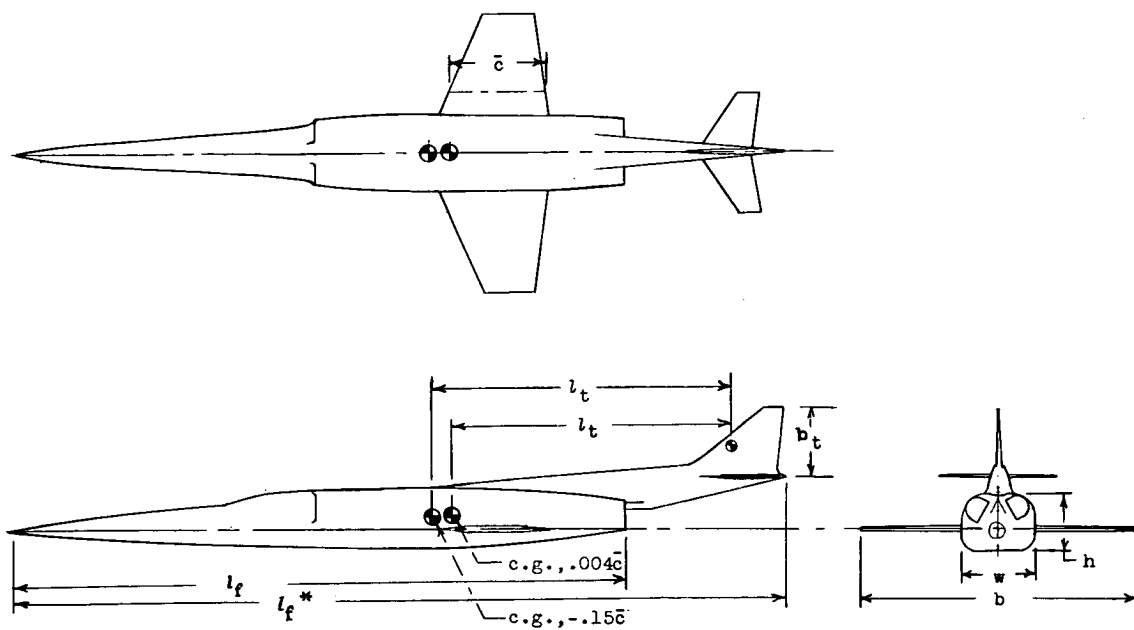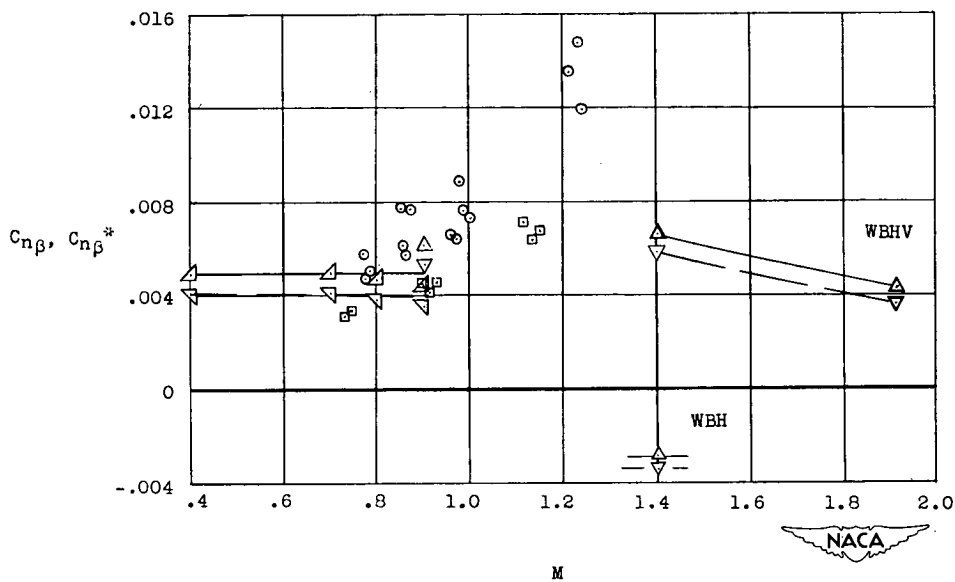
Figure 2.- Directional-stability data for model 1.
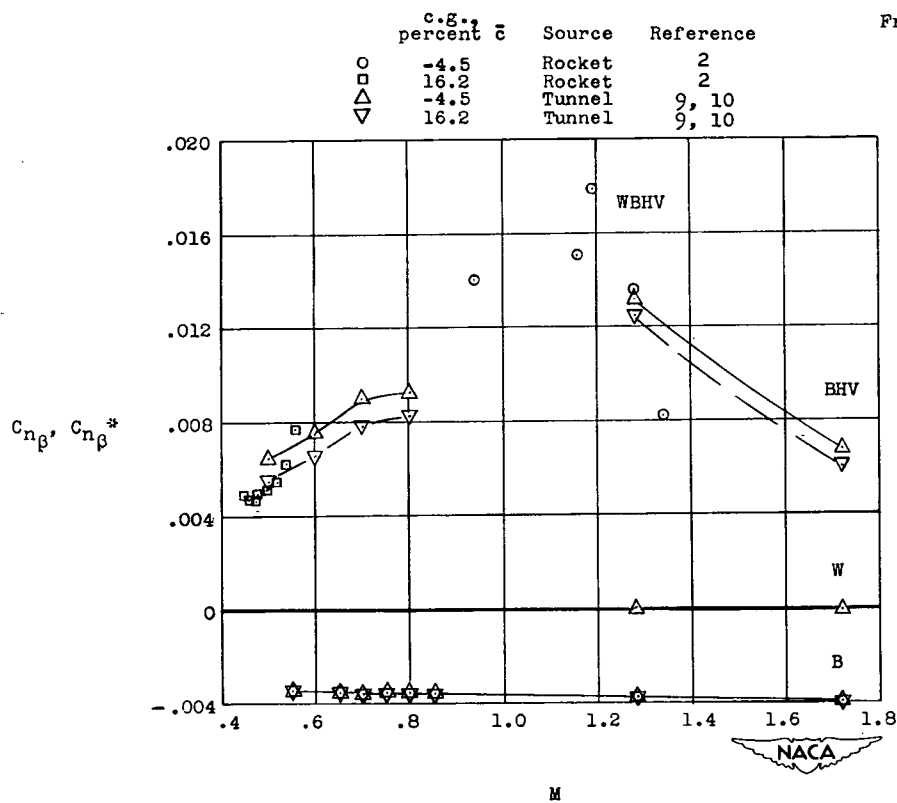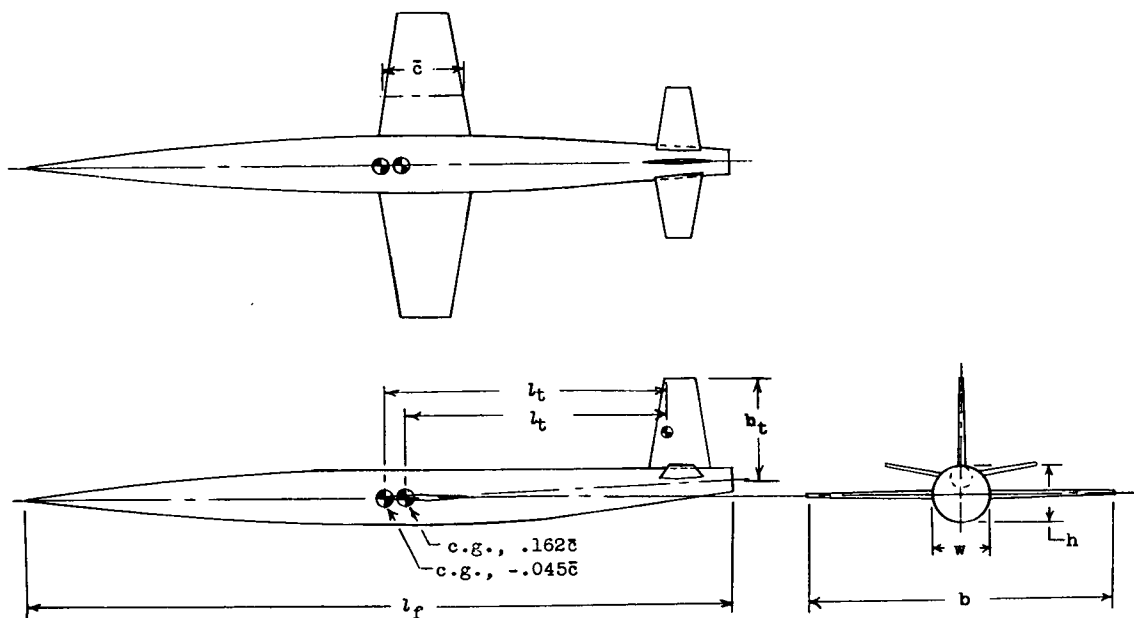
Figure 3.- Directional-stability data for model 2.
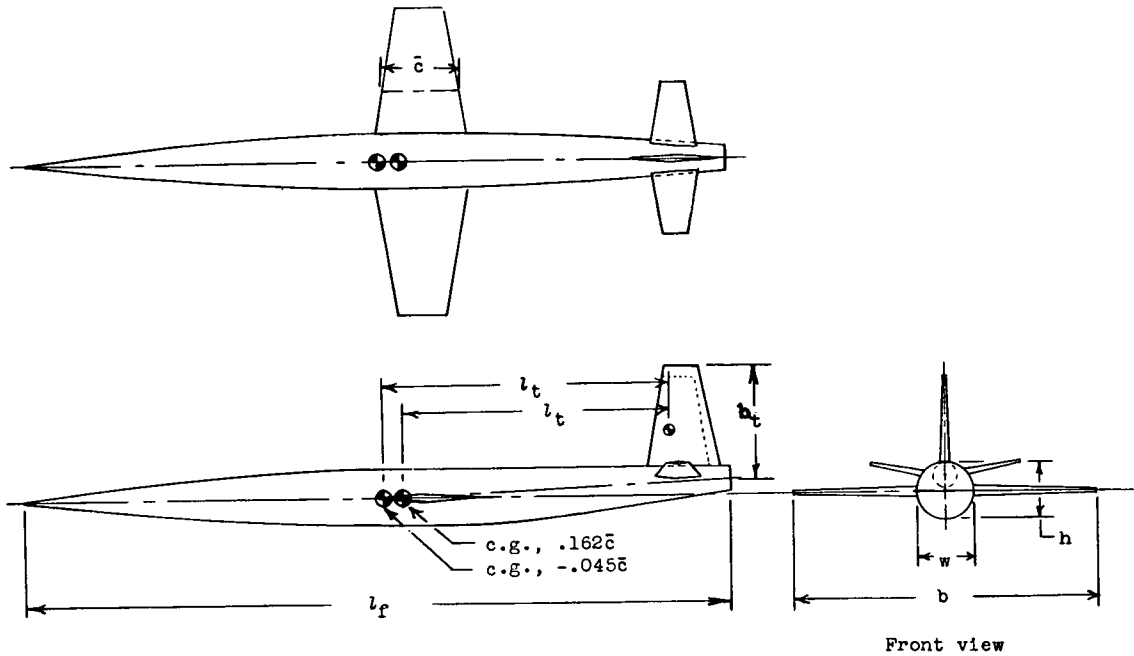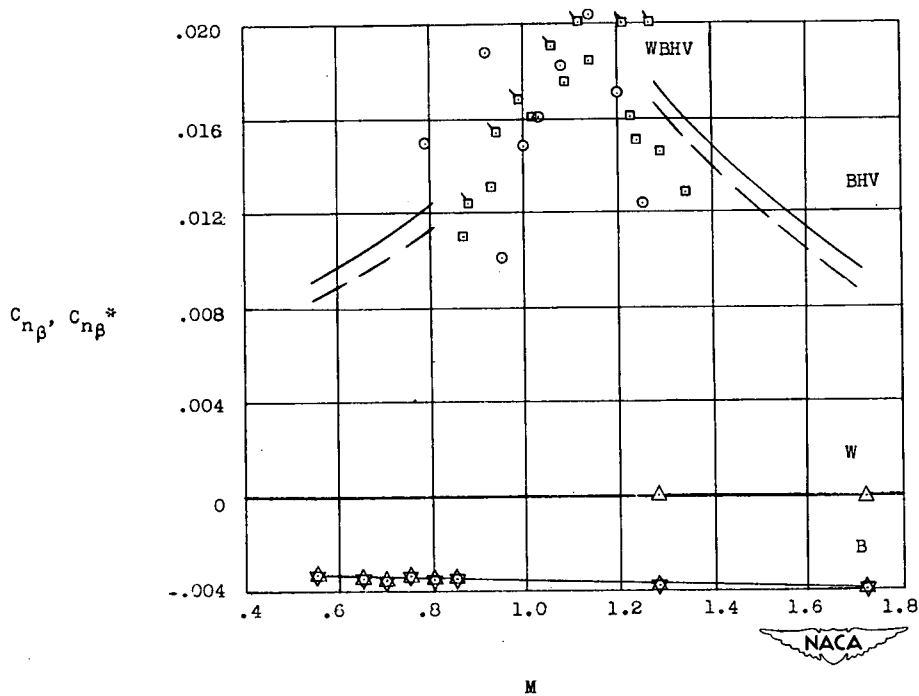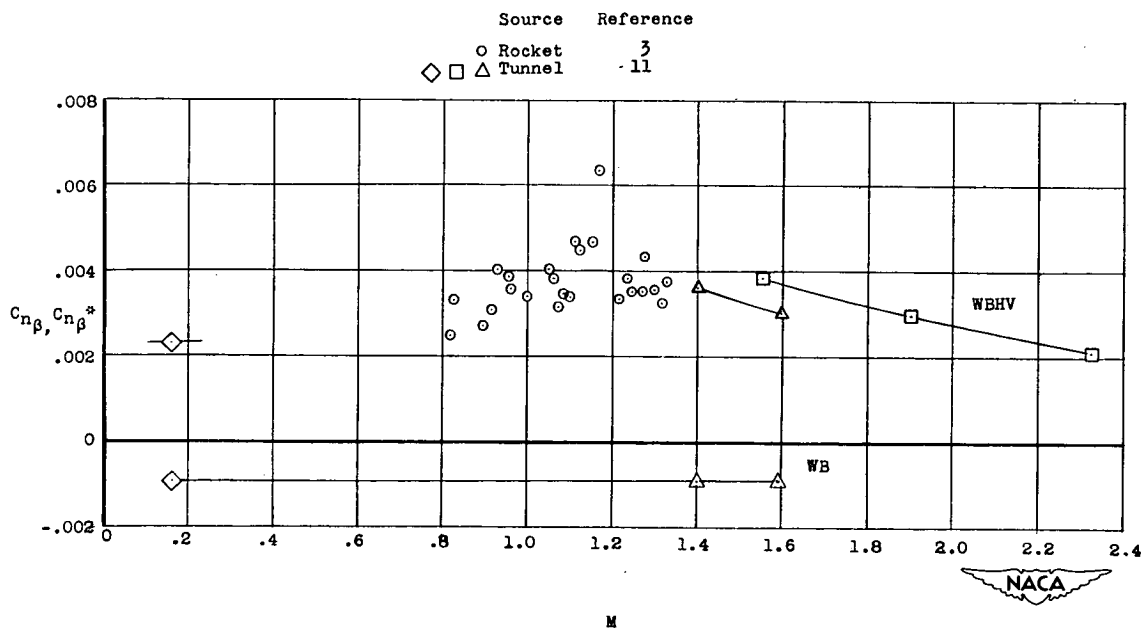
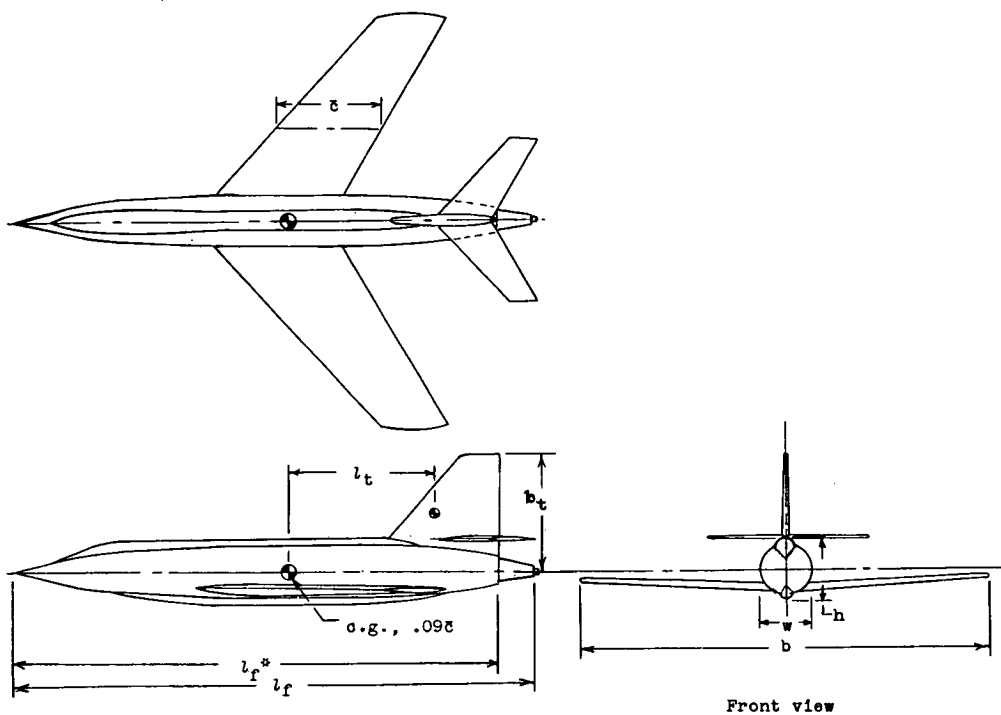Figure 4.- Directional-stability data for model 3.

Figure 5.- Directional-stability data for model 4.

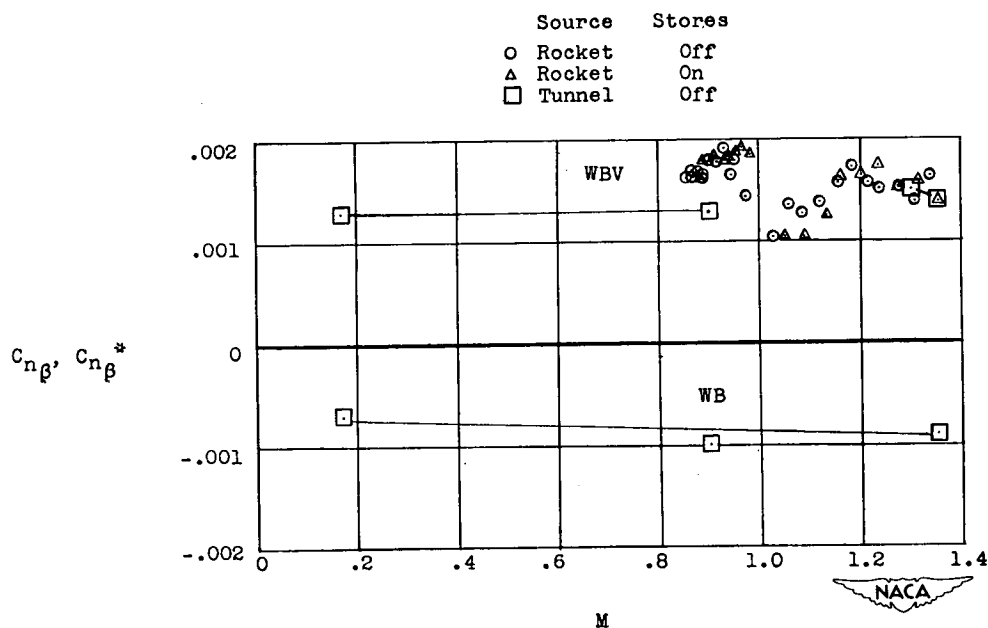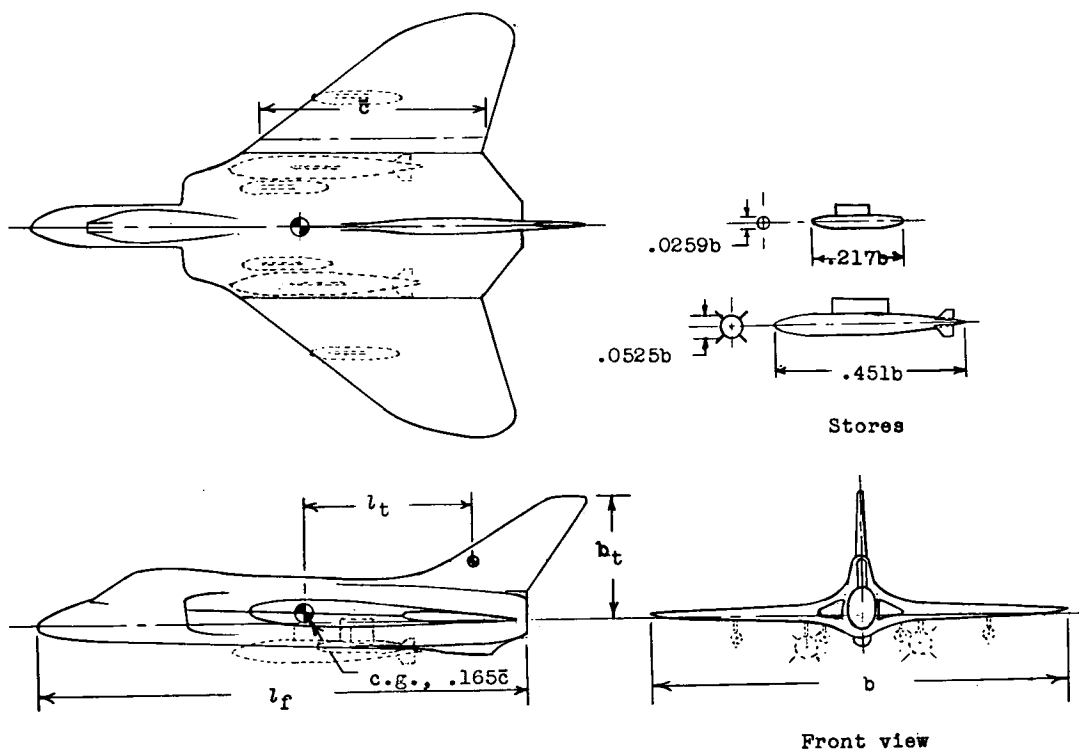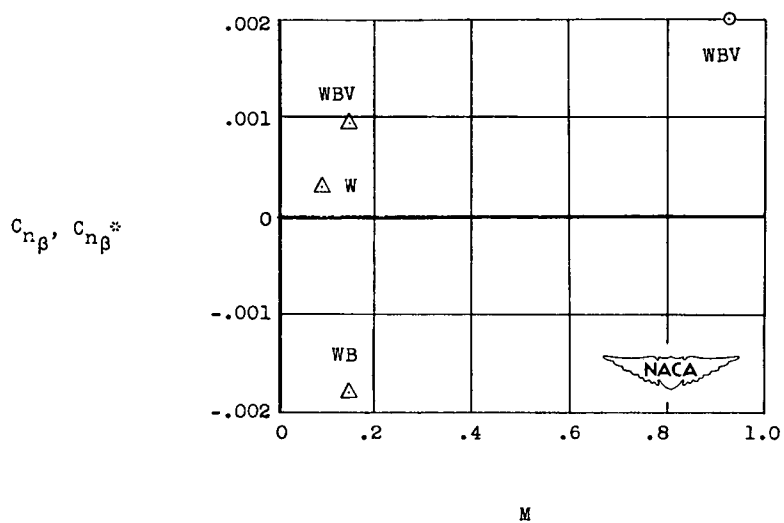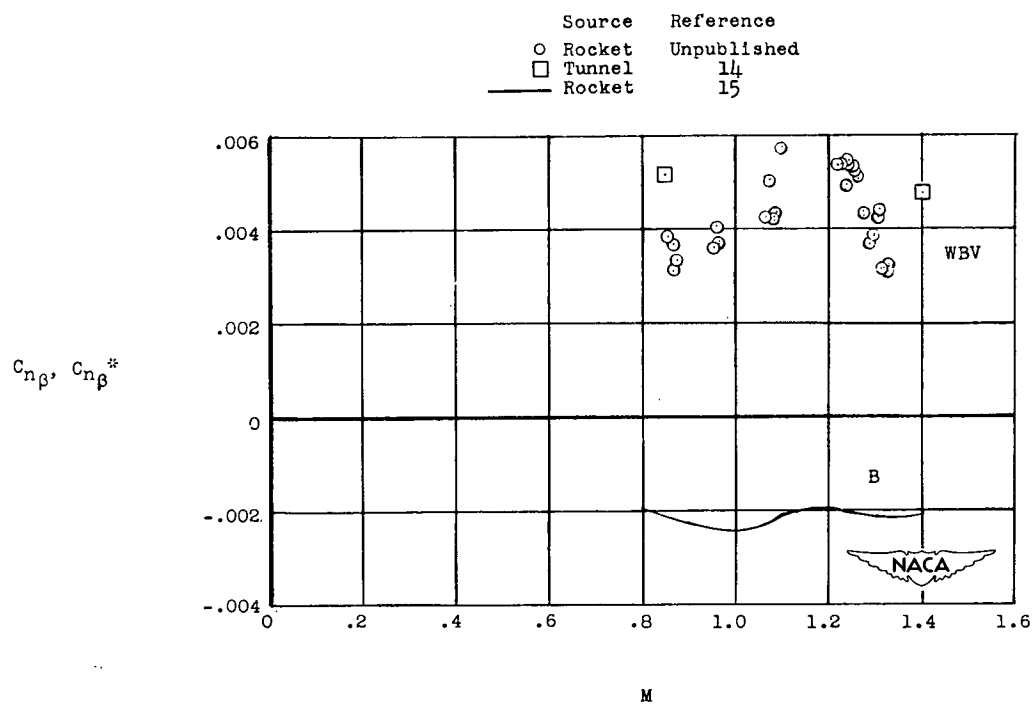Figure 6.- Directional-stability data for model 5, from unpublished
sources.
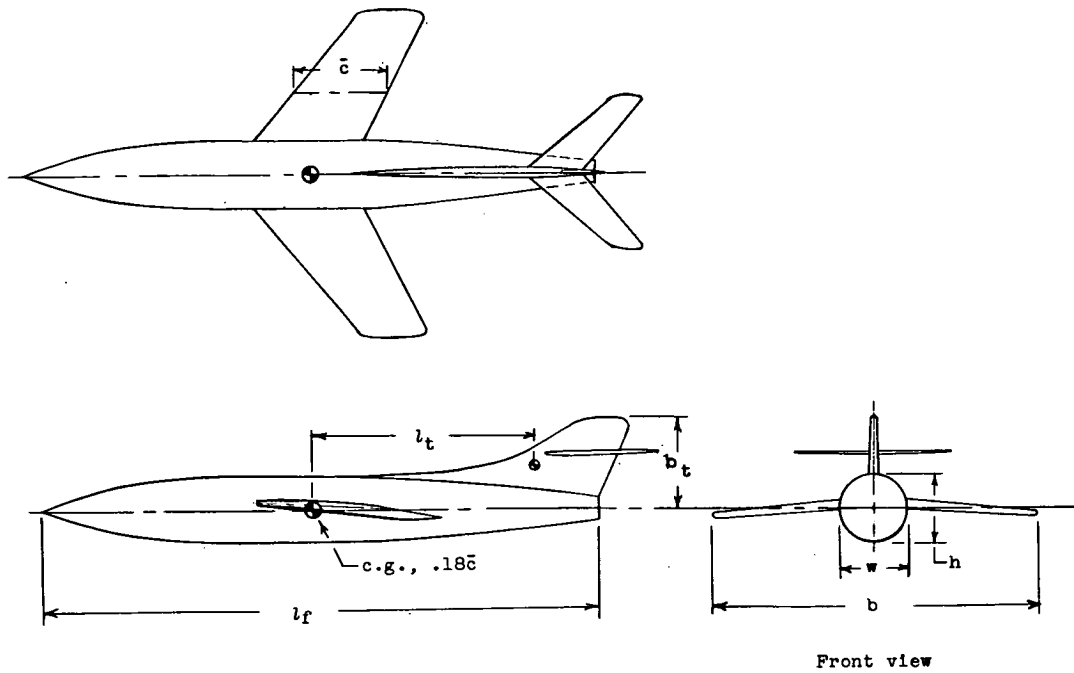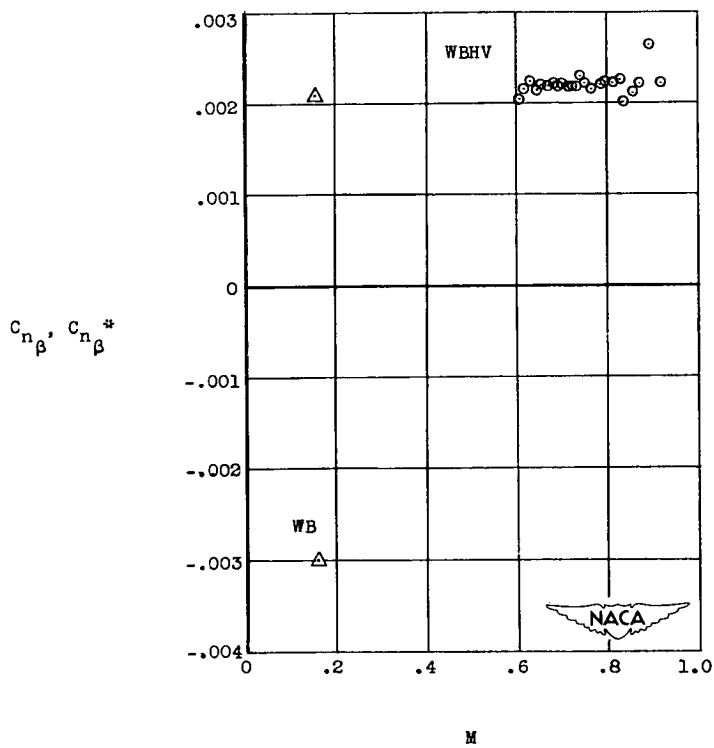
Figure 7.- Directional-stability data for model 6.
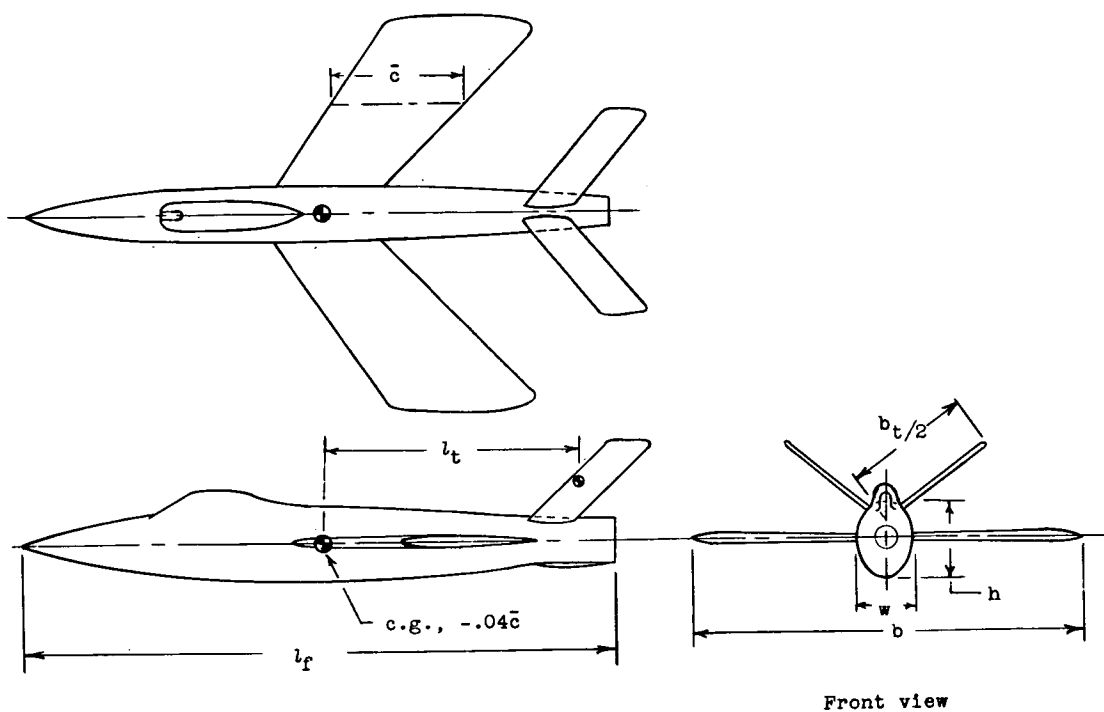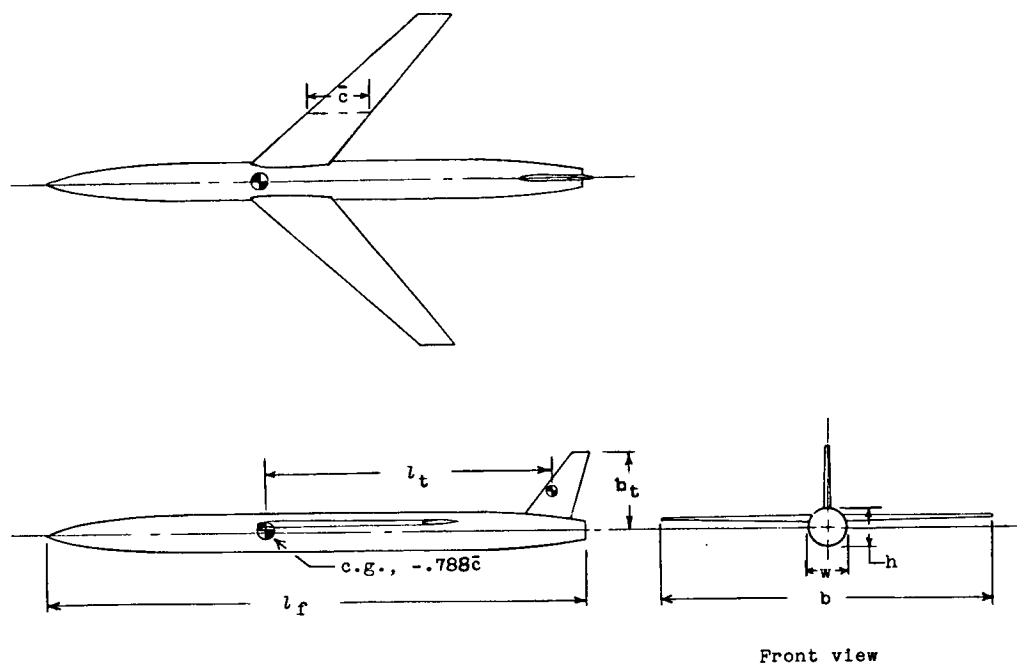
Figure 8.- Directional-stability data for model 7.

Figure 9.- Directional-stability data for model 8.